Gain Scheduling of Full-Order Flux Observer for Sensorless PMSM Drives Considering Magnetic Spatial Harmonics

Jiwon Yoo, Inhwi Hwang, Yoon-Ro Lee, and Seung-Ki Sul
Department of Electrical and Computer Engineering
Seoul National University
Seoul, Korea
vicenteyoo@gmail.com, snuhwi96@gmail.com, dbsfh92@snu.ac.kr, and sulsk@plaza.snu.ac.kr

2021 IEEE Energy Conversion Congress and Exposition (ECCE) | 978-1-7281-5135-9/21/$31.00 ©2021 IEEE | DOI: 10.1109/ECCE47101.2021.9595161

***Abstract*— This paper analyzes the effect of gain scheduling in the full-order flux observer for sensorless PMSM drives. The analysis shows that the conventional gain scheduling with fixed pole locations is vulnerable to the magnetic spatial harmonics of PMSM, especially at low speeds. To reduce the spatial harmonic disturbance on the angle estimation, a complex-vector style gains scheduling is proposed in this paper. The proposed gain scheduling inherently provides the speed-adaptive pole allocation, and it can effectively filter out the spatial harmonics of PMSM. Besides, a notch filter tuned to the 6th order harmonics, the dominant harmonic component in most PMSMs, is cascaded to the full-order observer. Thanks to the speed adaptive pole allocation and the notch filter, the sensorless observer keeps its stability at 5% of the rated speed under 200% of the rated torque.**

Keywords*— Gain scheduling, permanent magnet synchronous motor, sensorless control, spatial harmonics.

I. Introduction

Permanent magnet synchronous motor (PMSM) has been widely used for various industrial applications. In PMSM drives, the rotor position information is required to conduct the field-oriented control (FOC) or direct torque control (DTC). Instead of installing a position sensor, which provokes economic and mechanical issues, the sensorless PMSM drives have been developed and successfully applied to various industries. The sensorless algorithms for PMSM drives are classified into two groups; Signal-injection-based methods [1], [2] and model-based methods [3]-[7]. Unlike the signal-injection-based methods that require an additional voltage margin for signal-injection, the model-based methods estimate the rotor position based on the fundamental electrical model of PMSM. And, it has been preferred in various industrial applications if there is no requirement of torque control at extremely low-speed operation.

However, the model-based methods suffer a low signal-to-noise ratio (SNR) problem at low speeds. The stator voltage information includes disturbances such as inverter nonlinearity effect and dc-link voltage sensing error. They could be more severe in the low-speed region, where the fundamental voltage magnitude is not large enough. Moreover, the magnetic spatial harmonics induce a harmonic voltage that complicates the accurate rotor position estimation [7], [8].

Meanwhile, a state observer is often used for estimating the rotor position in model-based methods. Among the various observer structures, many research works have developed full-order observers [3]-[6]. To stabilize the observer, [3] applied a *dq*-decoupling gain matrix. The *dq*-decoupling gain matrix cancels the cross-coupling term in the system matrix and sets the poles to the stable region.

This paper analyzes the generalized gain scheduling of the full-order flux observer for sensorless PMSM drives. The analysis reveals that the conventional *dq*-decoupling gain matrix in [3] could be vulnerable to the spatial harmonics of PMSM. Instead of the *dq*-decoupling gain matrix with fixed pole location, this paper proposes a complex-vector style gain matrix, stabilizing the flux observer without *dq*-decoupling. The proposed gain matrix adaptively migrates the pole location to filter out the magnetic spatial harmonics of target PMSM. In addition, the proposed full-order observer can be cascaded with a harmonic rejecting notch filter, which minimizes the effect of 6th order spatial harmonics that would be a dominant harmonic in most PMSMs. Thanks to the proposed gain scheduling and the notch filter, a PMSM under test can operate at 5% of the rated speed with 200% of the rated torque, less affected by the inductance variation from the spatial harmonics of PMSM. The effectiveness of the proposed method is verified with the simulation and experimental results.

II. Conventional Gain Scheduling of Full-Order Observer

The PMSM's electrical model at the rotor reference frame (RRF) can be expressed as follows.

$$\frac{d}{dt}\left(\mathbf{L}_{\mathbf{dqs}}\mathbf{i}^{\mathbf{r}}_{\mathbf{dqs}}\right) = -\omega_r \mathbf{J}\left(\mathbf{L}_{\mathbf{dqs}}\mathbf{i}^{\mathbf{r}}_{\mathbf{dqs}}\right) - \begin{bmatrix} 0 \\ \omega_r \lambda_f \end{bmatrix} + \mathbf{v}^{\mathbf{r}}_{\mathbf{dqs}} - R_s \mathbf{i}^{\mathbf{r}}_{\mathbf{dqs}} \quad (1)$$

where $\mathbf{J} = \begin{bmatrix} 0 & -1 \\ 1 & 0 \end{bmatrix}$, $\mathbf{L}_{\mathbf{dqs}} = \begin{bmatrix} L_{ds} & 0 \\ 0 & L_{qs} \end{bmatrix}$, and ω_r is the rotor speed. R_s, L_{ds}, L_{qs}, and λ_f denote the stator resistance, the *d*- and *q*-axis static inductances, and the flux linkage of the permanent-magnet, respectively. $\mathbf{v}^{\mathbf{r}}_{\mathbf{dqs}}$ and $\mathbf{i}^{\mathbf{r}}_{\mathbf{dqs}}$ are the stator voltage and current vector at RRF. If there is an error between the actual rotor angle θ_r and the estimated rotor angle $\hat{\theta}_r$, the PMSM model at the estimated RRF (ERRF) can be obtained

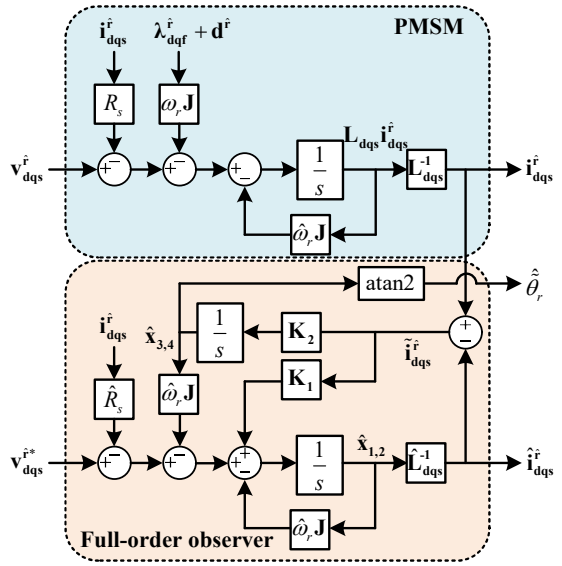

Fig. 1. Structure of full-order flux observer.

as follows by multiplying the rotational matrix $\mathbf{R}(\tilde{\theta}_r)=\cos(\tilde{\theta}_r)\mathbf{I}+\sin(\tilde{\theta}_r)\mathbf{J}$, where $\tilde{\theta}_r=\theta_r-\hat{\theta}_r$ and $\mathbf{I}=\begin{bmatrix}1 & 0\\ 0 & 1\end{bmatrix}$.

$$\frac{d}{dt}\boldsymbol{\lambda}^{\hat{\mathbf{r}}}_{\mathbf{dqi}}=-\omega_r\mathbf{J}\boldsymbol{\lambda}^{\hat{\mathbf{r}}}_{\mathbf{dqi}}-\omega_r\mathbf{J}\boldsymbol{\lambda}^{\hat{\mathbf{r}}}_{\mathbf{dqf}}+\mathbf{d}^{\hat{\mathbf{r}}}+\mathbf{v}^{\hat{\mathbf{r}}}_{\mathbf{dqs}}-R_s\mathbf{i}^{\hat{\mathbf{r}}}_{\mathbf{dqs}}. \quad (2)$$

where $\boldsymbol{\lambda}^{\hat{\mathbf{r}}}_{\mathbf{dqi}}=\mathbf{L}_{\mathbf{dqs}}\mathbf{i}^{\hat{\mathbf{r}}}_{\mathbf{dqs}}$, $\boldsymbol{\lambda}^{\hat{\mathbf{r}}}_{\mathbf{dqf}}=\begin{bmatrix}\lambda_f\cos(\tilde{\theta}_r)\\ \lambda_f\sin(\tilde{\theta}_r)\end{bmatrix}$, and $\omega_{\hat{r}}=\frac{d}{dt}\hat{\theta}_r$. $\mathbf{d}^{\hat{\mathbf{r}}}$ is the leftover term from the saliency of inductance, $\Delta L_s=0.5\cdot(L_{ds}-L_{qs})$. The detailed expression of $\mathbf{d}^{\hat{\mathbf{r}}}$ is written in the bottom of the page. In (3), $\mathbf{I_p}$ and $\mathbf{J_p}$ denote $\begin{bmatrix}1 & 0\\ 0 & -1\end{bmatrix}$ and $\begin{bmatrix}0 & 1\\ 1 & 0\end{bmatrix}$, respectively. From (2), a full-order observer taking $\mathbf{x}=\begin{bmatrix}x_1 & x_2 & x_3 & x_4\end{bmatrix}^T=\begin{bmatrix}\boldsymbol{\lambda}^{\hat{\mathbf{r}}}_{\mathbf{dqi}}\\ \boldsymbol{\lambda}^{\hat{\mathbf{r}}}_{\mathbf{dqf}}\end{bmatrix}$ as a state variable can be constructed as follows.

$$\frac{d}{dt}\hat{\mathbf{x}}=\hat{\mathbf{A}}\hat{\mathbf{x}}+\begin{bmatrix}\mathbf{I}\\ 0\end{bmatrix}\left(\mathbf{v}^{\hat{\mathbf{r}}}_{\mathbf{dqs}}-\hat{R}_s\mathbf{i}^{\hat{\mathbf{r}}}_{\mathbf{dqs}}\right)+\mathbf{K_o}\left(\mathbf{i}^{\hat{\mathbf{r}}}_{\mathbf{dqs}}-\hat{\mathbf{i}}^{\hat{\mathbf{r}}}_{\mathbf{dqs}}\right), \quad (4)$$

where

$$\hat{\mathbf{A}}=\begin{bmatrix}-\hat{\omega}_r\mathbf{J} & -\hat{\omega}_r\mathbf{J}\\ 0 & 0\end{bmatrix}. \quad (5)$$

The superscript "^" stands for the estimated variable, e.g., $\hat{\omega}_r$ and $\hat{R}_s$ are the estimated rotor speed and the estimated stator resistance used. The estimated current $\hat{\mathbf{i}}^{\hat{\mathbf{r}}}_{\mathbf{dqs}}$ is obtained as follows.

$$\hat{\mathbf{i}}^{\hat{\mathbf{r}}}_{\mathbf{dqs}}=\hat{\mathbf{C}}\hat{\mathbf{x}}=\begin{bmatrix}\hat{\mathbf{L}}^{-1}_{\mathbf{dqs}} & \mathbf{0}\end{bmatrix}\hat{\mathbf{x}}. \quad (6)$$

Fig. 1 shows the structure of the full-order observer in (4). $\mathbf{K_1}$ and $\mathbf{K_2}$ are the two-by-two gain matrices, which compose $\mathbf{K_o}$ in (4), i.e., $\mathbf{K_o}=[\mathbf{K_1}\ \mathbf{K_2}]^T$. The estimated angle error $\tilde{\hat{\theta}}_r$ is calculated by applying the arctangent function to $\hat{x}_3$ and $\hat{x}_4$. Since the system matrix $\hat{\mathbf{A}}$ is marginally stable, $\mathbf{K_1}$ and $\mathbf{K_2}$ should be set appropriately to stabilize the observer. For a stable operation, $\hat{\mathbf{A}}-\mathbf{K_o}\hat{\mathbf{C}}$ should be Hurwitz, and the characteristic function of the observer will be $\det\left(s\mathbf{I_4}-\hat{\mathbf{A}}+\mathbf{K_o}\hat{\mathbf{C}}\right)$, where $\mathbf{I_4}$ is the four-by-four identity matrix.

In [3], a *dq*-decoupling gain matrix was used. $\mathbf{K_1}$ and $\mathbf{K_2}$ are set as follows.

$$\mathbf{K}_{\mathbf{o,conv}}=\begin{bmatrix}\mathbf{K}_{\mathbf{1,conv}}\\ \mathbf{K}_{\mathbf{2,conv}}\end{bmatrix}=\begin{bmatrix}\left(2\zeta\omega_o\mathbf{I}-\hat{\omega}_r\mathbf{J}\right)\hat{\mathbf{L}}_{\mathbf{dqs}}\\ \left(\omega_o^2/\hat{\omega}_r\right)\mathbf{J}\hat{\mathbf{L}}_{\mathbf{dqs}}\end{bmatrix}. \quad (7)$$

With $\mathbf{K_{o,conv}}$, $\det(s\mathbf{I_4}-\hat{\mathbf{A}}+\mathbf{K_{o,conv}}\hat{\mathbf{C}})$ is calculated as follows.

$$\det\left(s\mathbf{I_4}-\hat{\mathbf{A}}+\mathbf{K_{o,conv}}\hat{\mathbf{C}}\right)=\left(s^2+2\zeta\omega_o s+\omega_o^2\right)^2. \quad (8)$$

Therefore, the observer would be stable for a positive ω_o and ζ. The error dynamics of $\tilde{\mathbf{x}}=\mathbf{x}-\hat{\mathbf{x}}$ would be calculated as follows, assuming accurate motor parameters and rotor speed.

$$\frac{d}{dt}\tilde{\mathbf{x}}=\begin{bmatrix}-2\zeta\omega_o\mathbf{I} & -\hat{\omega}_r\mathbf{J}\\ -\dfrac{\omega_o^2}{\hat{\omega}_r}\mathbf{J} & 0\end{bmatrix}\tilde{\mathbf{x}}. \quad (9)$$

Eq. (9) can be separated with two independent dynamics as follows.

$$\frac{d}{dt}\begin{bmatrix}\tilde{x}_1\\ \tilde{x}_4\end{bmatrix}=\begin{bmatrix}-2\zeta\omega_o & -\hat{\omega}_r\\ -\omega_o^2/\hat{\omega}_r & 0\end{bmatrix}\begin{bmatrix}\tilde{x}_1\\ \tilde{x}_4\end{bmatrix}. \quad (10)$$

$$\frac{d}{dt}\begin{bmatrix}\tilde{x}_2\\ \tilde{x}_3\end{bmatrix}=\begin{bmatrix}-2\zeta\omega_o & \hat{\omega}_r\\ \omega_o^2/\hat{\omega}_r & 0\end{bmatrix}\begin{bmatrix}\tilde{x}_2\\ \tilde{x}_3\end{bmatrix}. \quad (11)$$

Since $\tilde{x}_1$ in (10) is $\tilde{\lambda}^{\hat{r}}_{di}=\lambda^{\hat{r}}_{di}-\hat{\lambda}^{\hat{r}}_{di}$, the dynamic equation in (10) stands for the *d*-axis flux dynamics. By the same way, (11) represents the *q*-axis flux dynamics.

III. Proposed Gain Scheduling

A. Generalized Stabilizing Gain Analysis

$\det(s\mathbf{I_4}-\hat{\mathbf{A}}+\mathbf{K_o}\hat{\mathbf{C}})$ can be expressed with an arbitrary gain matrix. The gain matrices, $\mathbf{K_1}$ and $\mathbf{K_2}$, are rewritten as follows.

$$\begin{bmatrix}\mathbf{K_1}\\ \mathbf{K_2}\end{bmatrix}=\begin{bmatrix}\mathbf{K_1'}\hat{\mathbf{L}}_{\mathbf{dqs}}\\ \mathbf{K_2'}\hat{\mathbf{L}}_{\mathbf{dqs}}\end{bmatrix}, \quad (12)$$

where $\mathbf{K_1'}=k_{11}\mathbf{I}+k_{12}\mathbf{J}$ and $\mathbf{K_2'}=k_{21}\mathbf{I}+k_{22}\mathbf{J}$. Applying (12), $\det(s\mathbf{I_4}-\hat{\mathbf{A}}+\mathbf{K_o}\hat{\mathbf{C}})$ can be calculated as follows.

$$\mathbf{d}^{\hat{\mathbf{r}}}=-\frac{1}{\omega_r}\left(\omega_{\hat{r}}\Delta L_s\sin 2\tilde{\theta}_r\mathbf{I_p}\mathbf{i}^{\hat{\mathbf{r}}}_{\mathbf{dqs}}+\omega_{\hat{r}}\Delta L_s(1-\cos 2\tilde{\theta}_r)\mathbf{J_p}\mathbf{i}^{\hat{\mathbf{r}}}_{\mathbf{dqs}}-\frac{d}{dt}\left(\Delta L_s\sin 2\tilde{\theta}_r\mathbf{J_p}\mathbf{i}^{\hat{\mathbf{r}}}_{\mathbf{dqs}}\right)+\frac{d}{dt}\left(\Delta L_s(1-\cos 2\tilde{\theta}_r)\mathbf{I_p}\mathbf{i}^{\hat{\mathbf{r}}}_{\mathbf{dqs}}\right)\right). \quad (3)$$

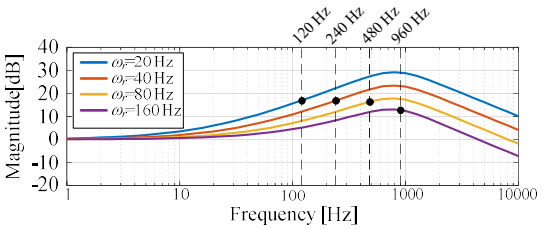

Fig. 2. Bode plot of $\mathbf{H}_{\mathbf{L,conv}}$.

$$\det\left(s\mathbf{I}_4-\hat{\mathbf{A}}+\mathbf{K}_o\hat{\mathbf{C}}\right)=\det\left(s^2\mathbf{I}+s\hat{\omega}_r\mathbf{J}+s\mathbf{K}_1^{'}-\hat{\omega}_r\mathbf{J}\mathbf{K}_2^{'}\right). \quad (13)$$

The stability of the observer can be evaluated by solving $\det(s^2\mathbf{I}+s\hat{\omega}_r\mathbf{J}+s\mathbf{K}_1^{'}-\hat{\omega}_r\mathbf{J}\mathbf{K}_2^{'})=0$. However, (13) is a fourth-order polynomial, which is hard to be intuitively solved. Fortunately, the determinant of a matrix consisting of **I** and **J** can be calculated through a complex-number-coefficient equation. Substituting **I** and **J** in (13) with real unit 1 and imaginary unit *j*, (13) can be transformed as follows.

$$s^2+\hat{\omega}_r js+s\mathbf{k}_1-\hat{\omega}_r j\mathbf{k}_2=0, \quad (14)$$

where $\mathbf{k}_1=k_{11}+k_{12}j$, $\mathbf{k}_2=k_{21}+k_{22}j$. It is known that solving (13) is equivalent to solving (14). Hence, the roots of $\det(s^2\mathbf{I}+s\hat{\omega}_r\mathbf{J}+s\mathbf{K}_1^{'}-\hat{\omega}_r\mathbf{J}\mathbf{K}_2^{'})=0$ are the same as roots of (14) and their conjugates.

Assuming the observer's stable operation, the final convergence point can be calculated as follows under the presence of the parameter errors. If there are errors in L_{ds} and L_{qs}, the estimated state $\hat{\mathbf{x}}$ would differ from the actual state **x**, as (15). In (15), $\tilde{\mathbf{\Gamma}}$ represents the inductance error ratio, i.e., $\tilde{\mathbf{\Gamma}}=(\mathbf{L}_{\mathbf{dqs}}-\hat{\mathbf{L}}_{\mathbf{dqs}})\mathbf{L}_{\mathbf{dqs}}^{-1}$. For *dq*-decoupling gain matrix in (7), $\hat{x}_3$ and $\hat{x}_4$ can be rewritten as follows.

$$\begin{bmatrix}\hat{x}_3\\ \hat{x}_4\end{bmatrix}=\mathbf{H}_{\mathbf{F,conv}}\left(\begin{bmatrix}\lambda_f\cos(\tilde{\theta}_r)\\ \lambda_f\sin(\tilde{\theta}_r)\end{bmatrix}+\mathbf{d}^{\hat{\mathbf{r}}}\right)+\mathbf{H}_{\mathbf{L,conv}}\begin{bmatrix}\tilde{L}_{ds}i_{ds}^{\hat{r}}\\ \tilde{L}_{qs}i_{qs}^{\hat{r}}\end{bmatrix}, \quad (16)$$

where

$$\mathbf{H}_{\mathbf{F,conv}}=\frac{\omega_o^{\,2}}{s^2+2\zeta\omega_o s+\omega_o^{\,2}}, \quad (17)$$

$$\mathbf{H}_{\mathbf{L,conv}}=\frac{\omega_o^{\,2}}{s^2+2\zeta\omega_o s+\omega_o^{\,2}}\left(s\frac{\mathbf{J}}{\hat{\omega}_r}-\mathbf{I}\right). \quad (18)$$

$\mathbf{H}_{\mathbf{F,conv}}$ is the transfer function estimating the flux linkage of the permanent magnet. $\mathbf{H}_{\mathbf{L,conv}}$ is the effect of the disturbance on the flux estimation. Fig. 2 shows Bode plots of $\mathbf{H}_{\mathbf{L,conv}}$ at various rotor speeds of a PMSM under study. The PMSM is a 1.7 kW-rated interior PMSM (IPMSM), of which parameters are listed in TABLE I. In Fig. 2, ω_o and ζ are set as $2\pi\cdot800$ rad/s and 1, respectively. $\tilde{\mathbf{\Gamma}}$ includes not only the average inductance errors, but also the inductance variation due to spatial harmonics. Thus, the effect of the *h*-th order spatial harmonics can be evaluated with $\mathbf{H}_{\mathbf{L,conv}}(jh\hat{\omega}_r)$. For a healthy PMSM, the lowest order of the spatial harmonics would be the sixth, i.e. *h*=6. In Fig. 2, $\mathbf{H}_{\mathbf{L,conv}}(j6\hat{\omega}_r)$ at each speed is denoted as black dot.

TABLE I. Motor parameters

Rated power	1.7	kW
Rated torque	4.5	N·m
Rated current	5.2	A_{rms}
DC-link voltage	311	V_{dc}
Pole/slot	8 / 9	
λ_f	88.4	mWb·t
L_{ds} @ T_e=2 p.u.	6.3	mH
L_{qs} @ T_e=2 p.u.	8.5	mH

Since the 6th order harmonics are not attenuated at low speeds, it would generate a substantial ripple in the angle estimation. Therefore, the *dq*-decoupling gain with fixed pole location would be vulnerable to the spatial harmonics, especially at low speeds. To mitigate the adverse effect of spatial harmonics, the complex vector style gain scheduling with speed-adaptive pole allocation is proposed in this paper.

B. Complex Vector Style Gain Scheduling

In (14), the stabilizing gain $\mathbf{k}_1$ and $\mathbf{k}_2$ can be selected as follows.

$$\mathbf{k}_1=\omega_o+a|\hat{\omega}_r|, \quad (19)$$

$$\mathbf{k}_2=-\omega_o\left(1-a\,\mathrm{sgn}(\hat{\omega}_r)j\right), \quad (20)$$

where ω_o and a are positive real numbers. The function 'sgn(x)' stands for the sign of x, as follows.

$$\mathrm{sgn}(\mathrm{x})=\begin{cases}1, & for\ \mathrm{x}\ge 0,\\ -1, & for\ \mathrm{x}<0.\end{cases} \quad (21)$$

The roots of (14) can be calculated as $-\omega_o$ and $-\left(a|\hat{\omega}_r|+\hat{\omega}_r j\right)$, and the system will be stable except for $\hat{\omega}_r=0$. The error dynamics would be calculated as follows.

$$\frac{d}{dt}\tilde{\mathbf{x}}=\begin{bmatrix}-\left(\omega_o+a|\hat{\omega}_r|\right)\mathbf{I}-\hat{\omega}_r\mathbf{J} & -\hat{\omega}_r\mathbf{J}\\ \omega_o\mathbf{I}-\omega_o a\,\mathrm{sgn}(\hat{\omega}_r)\mathbf{J} & 0\end{bmatrix}\tilde{\mathbf{x}}. \quad (22)$$

From (22), $\hat{x}_3$ and $\hat{x}_4$ can be calculated under the inductance errors as follows.

$$\begin{bmatrix}\hat{x}_3\\ \hat{x}_4\end{bmatrix}=\mathbf{H}_{\mathbf{F,prop}}\left(\begin{bmatrix}\lambda_f\cos(\tilde{\theta}_r)\\ \lambda_f\sin(\tilde{\theta}_r)\end{bmatrix}+\mathbf{d}^{\hat{\mathbf{r}}}\right)+\mathbf{H}_{\mathbf{L,prop}}\begin{bmatrix}\tilde{L}_{ds}i_{ds}^{\hat{r}}\\ \tilde{L}_{qs}i_{qs}^{\hat{r}}\end{bmatrix}, \quad (23)$$

where

$$\mathbf{H}_{\mathbf{F,prop}}=\frac{\omega_o}{s+\omega_o}\frac{\mathbf{H}_1}{H_{ch}}, \quad (24)$$

$$\mathbf{H}_{\mathbf{L,prop}}=-\frac{\omega_o}{(s+\omega_o)}\frac{\mathbf{H}_1}{H_{ch}}\left(\frac{s}{\hat{\omega}_r}\mathbf{J}-\mathbf{I}\right), \quad (25)$$

$$\hat{\mathbf{x}}=\mathbf{x}+\left(s\mathbf{I}_4-\hat{\mathbf{A}}+\mathbf{K}_o\hat{\mathbf{C}}\right)^{-1}\left(\begin{bmatrix}\mathbf{0} & \mathbf{0}\\ \mathbf{0} & -s\mathbf{I}\end{bmatrix}-\begin{bmatrix}\mathbf{K}_1^{'}\tilde{\mathbf{\Gamma}} & \mathbf{0}\\ \mathbf{K}_2^{'}\tilde{\mathbf{\Gamma}} & \mathbf{0}\end{bmatrix}\right)\mathbf{x}-\left(s\mathbf{I}_4-\hat{\mathbf{A}}+\mathbf{K}_o\hat{\mathbf{C}}\right)^{-1}\begin{bmatrix}\omega_r\mathbf{J}\\ \mathbf{0}\end{bmatrix}\mathbf{d}^{\hat{\mathbf{r}}}. \quad (15)$$

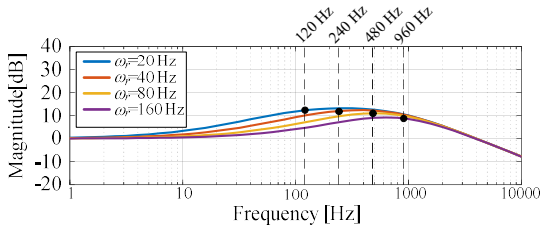

Fig. 3. Bode plot of $\mathbf{H}_{\mathbf{L,prop}}$.

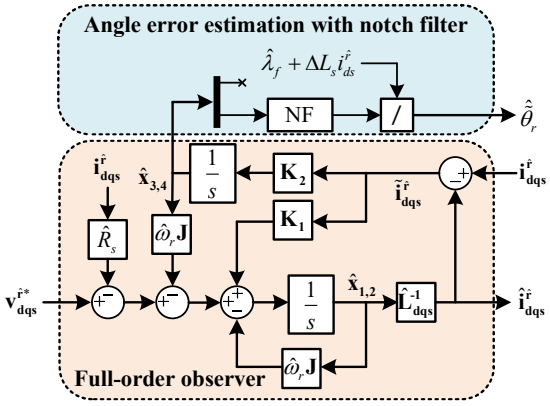

Fig. 4. Full-order observer with 6th order harmonic elimination.

$$\mathbf{H}_1 = \left(s\left(a\left|\hat{\omega}_r\right|\right)\mathbf{I} + \hat{\omega}_r\mathbf{J}\right) + \left(a^2+1\right)\hat{\omega}_r{}^2\mathbf{I}\right), \tag{26}$$

$$H_{ch} = \left(s^2 + 2a\left|\hat{\omega}_r\right|s + \left(a^2+1\right)\hat{\omega}_r{}^2\right). \tag{27}$$

Observing (24) and (25), ω_o determines the bandwidth of overall low pass filters on the observer. Unlike the *dq*-decoupling gain scheduling, $\mathbf{H}_{\mathbf{L,prop}}$ has $\mathbf{H}_1/H_{ch}$, which is a speed-adaptive low-pass filter. To attenuate the effect of 6th order harmonics, a should be less than 6. However, since an excessively small a would limit the dynamic performance of the observer, a trade-off should be made when determining the range of a. In this paper, ω_o and a are set as $2\pi 800$ rad/s and 5, respectively. Fig. 3 shows the Bode plot of $\mathbf{H}_{\mathbf{L,prop}}$. Thanks to the speed-adaptive pole $-\left(a\left|\hat{\omega}_r\right| + \hat{\omega}_r j\right)$, $\mathbf{H}_{\mathbf{L,prop}}\left(j6\hat{\omega}_r\right)$ has a lower magnitude than that of $\mathbf{H}_{\mathbf{L,conv}}\left(j6\hat{\omega}_r\right)$ in Fig. 2 at each speed, at least by 5 dB.

If an additional disturbance rejection performance is required, reducing a would be an option. However, as aforementioned, it will also limit the bandwidth of $\mathbf{H}_{\mathbf{F,prop}}$, which determines the dynamic performance of the observer. To minimize the effect of the spatial harmonics, a 6th order harmonic notch filter can be cascaded in the angle error estimation, as depicted in Fig. 4. NF block denotes 6th order harmonic notch filter.

For the 6th order harmonic notch filter, the harmonic flux harmonic in [8], depicted in Fig. 5, can be adopted. Fig. 6 shows the Bode plot of $\mathbf{H}_{\mathbf{F,prop}}$, including the effect of a notch filter. In Fig. 6, ζ_n of the notch filter is set as 0.1. With the notch filter, 6th order harmonic can be almost eliminated without deterioration in the observer bandwidth.

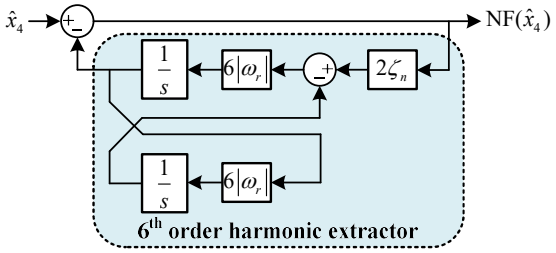

Fig. 5. Structure of 6th order harmonic notch filter.

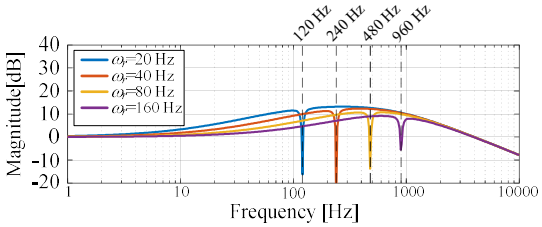

Fig. 6. Bode plot of $\mathbf{H}_{\mathbf{L,prop}}$ including notch filter.

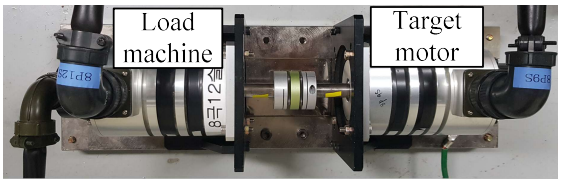

Fig. 7. Experimental setup

IV. Simulation and Experimental Results

A. Implementation

To verify the effectiveness of the proposed gain scheduling, simulation and experimental tests have been conducted. The 1.7 kW-rated IPMSM in Fig. 7 is selected for the motor under test, and its specification is listed in TABLE I. To see the effect of the spatial harmonics in simulation, the high-fidelity motor model in [9] is implemented. The flux map used in the simulation has been obtained through FEA results.

In the simulation and experiments, the load machine regulates the shaft speed, and the motor under test operates in torque control mode. The overall control block diagram is shown in Fig. 8. The current reference is calculated from the torque reference T_e^*, assuming maximum torque per Ampere (MTPA) operation. For the current regulator, the state-feedback type PI current regulator has been used, and its bandwidth is set as 200 Hz. To calculate $\hat{\theta}_r$ from $\hat{\tilde{\theta}}_r$, an extended state observer (ESO) has been adopted, of which bandwidth is set to 25 Hz. For the full-order observer, the gains are set equal to those used in Fig. 2 and Fig. 3, for the consistency with the analysis. Therefore, ω_o and ζ are set as $2\pi 800$ rad/s and 1, respectively, for the conventional gain setting. For the proposed gain setting, ω_o and a are set as $2\pi 800$ rad/s and 5, respectively. For the 6th order harmonic notch filter, ζ_n is set as 0.1.

B. Simulation Results

Fig. 9 (a)-(c) shows the simulation results. The target PMSM applies 200% of the rated torque, while the load

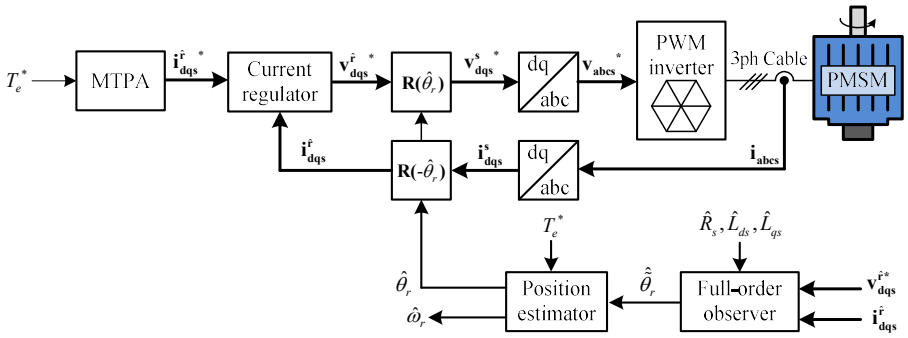

Fig. 8. Control block diagram.

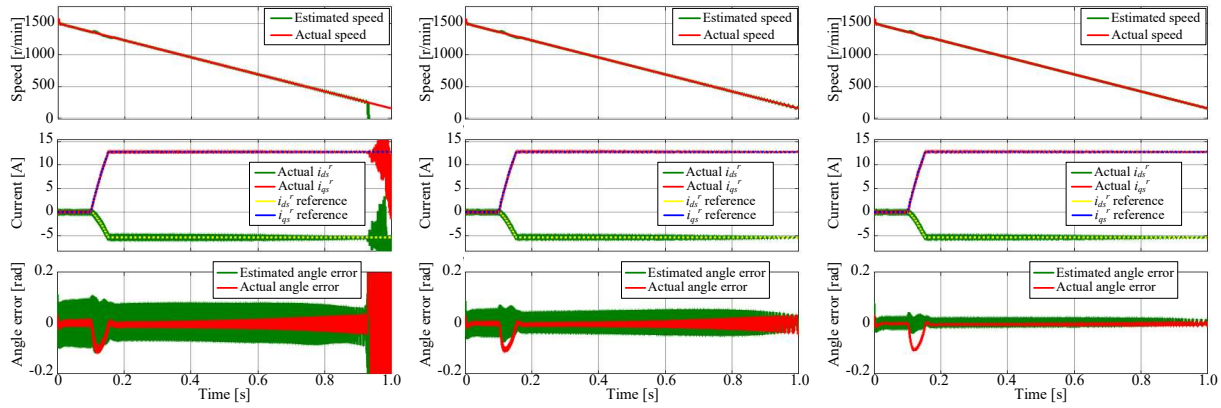

(a) (b) (c)

Fig. 9. Simulation Results. (a) Conventional gain scheduling. (b) Proposed gain scheduling. (c) Proposed gain with 6th order harmonic elimination.

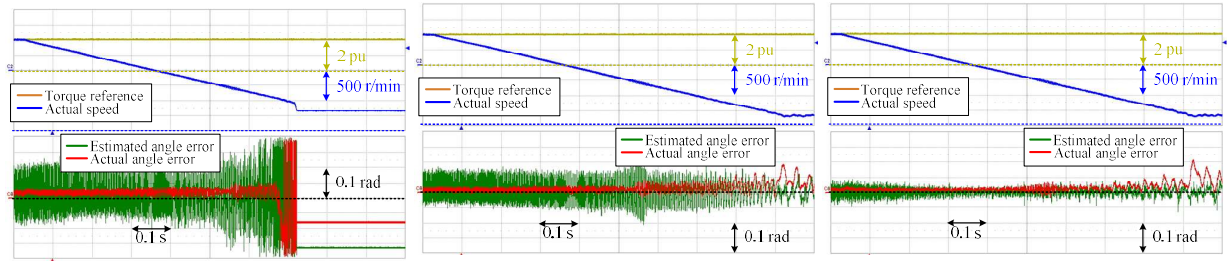

(a) (b) (c)

Fig. 10. Experimental Results. (a) Conventional gain scheduling. (b) Proposed gain scheduling. (c) Proposed gain with 6th order harmonic elimination.

machine regulates the speed. The initial speed reference is set as 1500 r/min, and it decreases up to 150 r/min. In Fig. 9 (a), the observer with the conventional decoupling gain scheduling suffers a considerable ripple in angle error estimation due to the spatial harmonics, and it loses stability at about 300 r/min. On the other hand, the proposed gain scheduling in Fig. 9 (b) keeps the stability even at 150 r/min, 5% of the rated speed, and the ripple in the angle error estimation is reduced to half as expected from the Bode plots. Fig. 9 (c) shows the simulation results of the proposed gain scheduling cascaded with the harmonic notch filter. Thanks to the notch filtering, 6th order harmonic components in angle estimation are eliminated. And, the angle error has been reduced conspicuously.

C. *Experimental Results*

The experimental results are shown in Fig. 10 (a)-(c). The experimental conditions correspond to those in the simulation. Similar to Fig. 9 (a), the conventional method loses its stability as the speed decreases, as shown in Fig. 10 (a). Unlike the simulation results, it can be noted that there is an irregular noise in the estimated angle error. It would arise from the practical uncertainties, e.g., mechanical asymmetry or voltage synthesis error, which have not been modelled in the simulation. In Fig. 10 (b), the effect of the spatial harmonics is effectively attenuated by the proposed gain scheduling, and the system keeps the stability even at 150 r/min. The major ripple, come from 6th order harmonics, in the estimated angle error can be eliminated by the additional notch filter, as shown in Fig. 10 (c).

V. Conclusion

This paper proposes a gain scheduling method for the full-order observer in sensorless PMSM drives. Unlike the conventional *dq*-decoupling gain scheduling, the proposed gain scheduling leaves the cross-coupling term as it is, and the pole locations are inherently changed according to the speed variation. The speed-adaptive pole allocation provides

the additional filtering effect on the spatial harmonics of PMSM, and the angle estimation performance in low-speed region can be enhanced. Moreover, the 6th order harmonic rejection notch filter is cascaded to the estimated flux linkage of the permanent magnet, which minimizes 6th order spatial harmonics on the angle estimation. The simulation and experimental results support the effectiveness of the proposed gain scheduling.

ACKNOWLEDGEMENT

This work was supported in part by the Hyundai Motor Chung Mong-Koo Foundation and in part by the BK21 FOUR program of the Education and Research Program for Future ICT Pioneers.

REFERENCES

[1] Y. -D. Yoon, S. -K. Sul, S. Morimoto and K. Ide, "High-Bandwidth Sensorless Algorithm for AC Machines Based on Square-Wave-Type Voltage Injection," in *IEEE Transactions on Industry Applications*, vol. 47, no. 3, pp. 1361-1370, May-June 2011.

[2] Y. -C. Kwon, J. Lee and S. -K. Sul, "Extending Operational Limit of IPMSM in Signal-Injection Sensorless Control by Manipulation of Convergence Point," in *IEEE Transactions on Industry Applications*, vol. 55, no. 2, pp. 1574-1586, March-April 2019.

[3] P. Kshirsagar *et al*., "Implementation and Sensorless Vector-Control Design and Tuning Strategy for SMPM Machines in Fan-Type Applications," in *IEEE Transactions on Industry Applications*, vol. 48, no. 6, pp. 2402-2413, Nov.-Dec. 2012.

[4] S. Po-ngam and S. Sangwongwanich, "Stability and Dynamic Performance Improvement of Adaptive Full-Order Observers for Sensorless PMSM Drive," in *IEEE Transactions on Power Electronics*, vol. 27, no. 2, pp. 588-600, Feb. 2012.

[5] Y. -C. Son, B. -H. Bae and S. -K. Sul, "Sensorless operation of permanent magnet motor using direct voltage sensing circuit," Conference Record of the 2002 *IEEE Industry Applications Conference. 37th IAS Annual Meeting* (Cat. No.02CH37344), Pittsburgh, PA, USA, 2002, pp. 1674-1678 vol.3.

[6] J. Yoo, Y. Lee and S. -K. Sul, "Back-EMF Based Sensorless Control of IPMSM with Enhanced Torque Accuracy Against Parameter Variation," *2018 IEEE Energy Conversion Congress and Exposition (ECCE)*, 2018, pp. 3463-3469.

[7] G. Zhang, G. Wang, D. Xu, R. Ni and C. Jia, "Multiple-AVF Cross-Feedback-Network-Based Position Error Harmonic Fluctuation Elimination for Sensorless IPMSM Drives," in *IEEE Transactions on Industrial Electronics*, vol. 63, no. 2, pp. 821-831, Feb. 2016.

[8] H. Kim, S. -K. Sul, H. Yoo and J. Oh, "Distortion-Minimizing Flux Observer for IPMSM Based on Frequency-Adaptive Observers," in *IEEE Transactions on Power Electronics*, vol. 35, no. 2, pp. 2077-2087, Feb. 2020, doi: 10.1109/TPEL.2019.2920691.

[9] X. Chen, J. Wang, B. Sen, P. Lazari and T. Sun, "A High-Fidelity and Computationally Efficient Model for Interior Permanent-Magnet Machines Considering the Magnetic Saturation, Spatial Harmonics, and Iron Loss Effect," in *IEEE Transactions on Industrial Electronics*, vol. 62, no. 7, pp. 4044-4055, July 2015.